Sugar-phosphate metabolism regulates stationary phase entry and stalk elongation in *Caulobacter crescentus*

Kevin D. de Young[1], Gabriele Stankeviciute[2], and Eric A. Klein[1,2,*]

[1]Biology Department, Rutgers University-Camden, Camden, NJ 08102

[2]Center for Computational and Integrative Biology, Rutgers University-Camden, Camden, NJ 08102

Running title: Sugar-phosphate metabolism regulates cell shape

Keywords: sugar-phosphate, cell shape, phosphate starvation, stationary phase, phosphomannose isomerase

[*]Correspondence:
Eric A. Klein
Department of Biology
Rutgers University-Camden
Camden, NJ 08102
eric.a.klein@rutgers.edu
Phone: (856) 225-6335
Fax: (856) 225-6312

Abstract

Bacteria have a variety of mechanisms for adapting to environmental perturbations. Changes in oxygen availability result in a switch between aerobic and anaerobic respiration, whereas iron limitation may lead to siderophore secretion. In addition to metabolic adaptations, many organisms respond by altering their cell shape. *Caulobacter crescentus*, when grown under phosphate limiting conditions, dramatically elongates its polar stalk appendage. The stalk is hypothesized to facilitate phosphate uptake; however, the mechanistic details of stalk synthesis are not well characterized. We used a chemical mutagenesis approach to isolate and characterize stalk-deficient mutants, one of which had two mutations in the phosphomannose isomerase gene (*manA*) that were necessary and sufficient to inhibit stalk elongation. Transcription of the *pho* regulon was unaffected in the *manA* mutant; therefore, ManA plays a unique regulatory role in stalk synthesis. The mutant ManA had reduced enzymatic activity resulting in a 5-fold increase in the intracellular fructose 6-phosphate: mannose 6-phosphate ratio. This metabolic imbalance impaired the synthesis of cellular envelope components derived from mannose 6-phosphate, namely lipopolysaccharide O-antigen and exopolysaccharide. Furthermore, the *manA* mutations prevented *C. crescentus* cells from efficiently entering stationary phase. Deletion of the stationary-phase response regulator *spdR* inhibited stalk elongation in wild-type cells while overproduction of the alarmone ppGpp, which triggers growth arrest and stationary phase entry, increased stalk length in the *manA* mutant strain. These results demonstrate that sugar-phosphate metabolism regulates stalk elongation independently of phosphate starvation.

Importance

Metabolic control of bacterial cell shape is an important mechanism for adapting to environmental perturbations. *Caulobacter crescentus* dramatically elongates its polar stalk appendage in response to phosphate starvation. To investigate the mechanism of this morphological adaptation, we isolated stalk-deficient mutants, one of which had mutations in the phosphomannose isomerase gene (*manA*) that blocked stalk elongation, despite normal activation of the phosphate-starvation response. The mutant ManA resulted in an imbalance in sugar-phosphate concentrations which had effects on the synthesis of cellular envelope components and entry into stationary phase. Due to the interconnectivity of metabolic pathways, our findings may suggest more generally that the modulation of bacterial cell shape involves the regulation of growth phase and the synthesis of cellular building blocks.

Introduction

The diversity of bacterial cell shapes found in nature highlights the selective pressure for maintaining particular morphologies. The Gram-negative Alphaproteobacteria, *Caulobacter crescentus*, forms a unipolar stalk appendage during its asymmetric cell cycle. The dimorphic life cycle of *C. crescentus* produces one motile (swarmer) cell and one adherent (stalked) cell at each cell cycle (1). The swarmer cell has a polar flagellum and pili and is replication-incompetent. The swarmer then sheds its flagellum and, at the same pole, produces a holdfast - the strongest measured biological adhesive (2). After the holdfast is secreted, the stalk is formed and elongated from the holdfast pole, thereby causing the holdfast to be pushed away from the cell body and localized to the tip of the stalk. This stalked cell can perform DNA replication in preparation for cell division. During cell division, a new flagellum is synthesized at the opposite pole. As a result, following cytokinesis, the stalked cell maintains its stalk and immediately re-enters the cell cycle, while the swarmer daughter cell is flagellated and enters a quiescent state from which it needs to emerge before synthesizing a new stalk and beginning a proliferative cycle.

In addition to its regulation by the cell cycle, stalk elongation is dramatically induced during phosphate limitation (3). Though the precise physiological functions of stalk elongation are not known, one proposed hypothesis was that the stalk acts as a “nutrient antenna” (4). Under the diffusive environment characteristic of freshwater lakes, nutrient flux is proportional to length; therefore, having a long thin appendage would be the most economical method of increasing cell length while minimizing surface area (5). Consistent with the “nutrient antenna” model, proteomic analysis of the stalk compartment found a large number of outer-membrane TonB-dependent receptors which facilitate the uptake of molecules into the periplasm (4). A

second proposed advantage of stalk elongation is that, in its natural environment, *C. crescentus* adheres to surfaces via holdfast at the stalk tip. By elongating the stalk, cells could extend away from the surface, exit the boundary layer, and gain access to convective fluid flow, where nutrients may be more available (6).

While the timing of stalk elongation and its physiological consequences are fairly well understood, we know comparatively little about the mechanism of stalk synthesis. The stalk is a true extension of the bacterial envelope containing inner- and outer-membranes as well as a peptidoglycan (PG) cell wall. The identification of PG synthesis proteins responsible for stalk elongation has been elusive. PG synthesis during cell elongation and septation is performed by a family of mono- and bi-functional penicillin-binding proteins (PBPs) that have transglycosylase and/or transpeptidase activities. Deletion of the *C. crescentus* transglycosylases either individually or in combination does not prevent stalk formation in low phosphate conditions (7, 8); any of the paralogs (except PbpZ) suffice for cellular growth and stalk biogenesis. These data suggest that either the redundancy of this activity allows any PBP to synthesize stalk PG or there is a yet unidentified enzyme required for stalk PG insertion. In contrast to the PG transglycosylases, inhibition of the transpeptidase PBP2 blocks stalk elongation (9, 10), as does depletion of MreB or RodA (11) which are regulators of PBP2 activity in *E. coli* (12, 13). Additionally, the stalk PG is enriched for LD-crosslinks (between *meso*-DAP residues on neighboring peptide stems) (9, 14); while these LD-crosslinks increase stalk PG resistance to lysozyme-mediated degradation (14), abrogation of LD-transpeptidation has no effect on stalk elongation (9, 14).

Studies using transposon mutagenesis or overexpression of fluorescent fusion proteins have successfully identified a number of stalk- or stalk-pole localized proteins, including: PbpC

106 (15), BacA (15), StpX (16), BamE (17), and DipM (18). The deletion of these genes shortens,
107 but does not eliminate, stalks in low-phosphate conditions. The difficulty in isolating a stalk-less
108 *C. crescentus* strain implies that either: 1) stalk synthesis is an essential physiological process, 2)
109 the synthesis enzymes have a secondary essential function and can therefore not be isolated by
110 transposon mutagenesis, or 3) there is redundancy in the stalk synthesis pathway.
111 In this report, we used chemical mutagenesis to introduce single-nucleotide
112 polymorphisms (SNPs) and screened for mutants with stalk elongation defects. We isolated a
113 strain with mutations in *ccna_03732* (*manA*), a phosphomannose isomerase, that affected sugar-
114 phosphate metabolism, cellular envelope biosynthesis, and entry into stationary phase. These
115 physiological perturbations decreased stalk length despite normal induction of the *pho* regulon,
116 suggesting that cellular metabolism regulates stalk elongation independently of phosphate
117 starvation.
118

Results

Isolation of a stalk-deficient mutant

Genetic screens for phenotypes of interest are commonly performed by transposon mutagenesis. While this approach is quite powerful and allows for easy mapping of transposon insertions, it has the drawback that insertions in essential genes are highly unlikely since these mutants tend to be total loss-of-function and lethal. As an alternative approach, we used chemical mutagenesis to introduce SNPs into the *C. crescentus* genome and devised a screening methodology to isolate stalk-deficient mutants (see Materials and Methods). Briefly, *C. crescentus* cells grown in Hutner-Imidazole-Glucose-Glutamate media (HIGG) containing 1 mM phosphate (high phosphate) were treated with 1-methyl-3-nitro-1-nitrosoguanidine (NTG) to induce DNA mutations. The cells were washed and resuspended in HIGG- 1 μM phosphate (low phosphate) to induce stalk elongation. To separate cells with stalk deficiencies, we reasoned that stalked cells float on top of a Percoll density gradient whereas non-stalked swarmer cells settle near the bottom of the gradient; therefore, we hypothesized that stalk-deficient cells would move to the bottom of a Percoll gradient. After 72 h of growth, cells were collected and subjected to three rounds of Percoll gradient centrifugation, each time collecting cells from the bottom of the gradient. Following the final gradient, cells were plated to isolate individual mutants. 384 individual colonies (4 x 96 well plates) were grown in HIGG- 1 μM phosphate and visually screened for stalk-phenotypes. We collected 4 mutants with clear phenotypes; three strains had short stalks of varying length and one strain had a stalk-shedding phenotype similar to that described for the NY111d1 isolate (19). One particular isolate, designated Stalk-Deficient-

Mutant 1 (SDM1) had very short stalks compared to wild-type when grown in low phosphate (Fig. 1A), and we focused on this strain in this work.

Mapping the SDM1 mutation

Whole-genome sequencing of the SDM1 strain yielded 79 potential SNPs. To identify the causative mutation for the stalk elongation phenotype, we performed complementation assays using a *C. crescentus* genomic cosmid library (20). Two cosmids, 2G12 and 2H1, were able to restore stalk elongation in low phosphate (Fig. 1A). These cosmids had an overlapping region of approximately 10 kb which contained 10 genes. Based on our sequencing data, of these 10 genes, only *ccna_03732* had any SNPs (Fig. 1B) and this gene is annotated as being in a single gene operon (21). The two missense mutations in *ccna_03732* resulted in amino acid substitutions A19T and G335N. To confirm that *ccna_03732* was necessary for the stalk elongation phenotype, we exogenously expressed wild-type *ccna_03732* in the SDM1 strain and observed recovery of stalk synthesis (Fig. 1C). Introduction of the two missense mutations into the *ccna_03732* chromosomal locus of wild-type *C. crescentus* phenocopied the SDM1 stalk deficiency, thereby demonstrating that these mutations were sufficient to inhibit stalk elongation (Fig. 1C). We often observed that the *ccna_03732*$^{A19T/G335N}$ appeared phase-bright (see Figs. 2E and 3D), suggesting a change in intracellular organization; however, the nature of this alteration is unknown. To determine which SNP was responsible for the SDM1 phenotype, we introduced each SNP individually into the *C. crescentus* chromosome; the A19T mutation had no significant effect on stalk elongation whereas the G335N mutation only partially recapitulated the elongation defect seen in SDM1 (Fig. 1C-D). Therefore, we conclude that the SDM1 stalk-elongation phenotype required both SNPs. The *ccna_03732* gene is predicted to be essential (22)

and we were unable to generate a deletion of this gene using standard allelic replacement methods, consistent with the gene's predicted essential functions. We tested whether the *ccna_03732* mutations affected the ability of *C. crescentus* to sense low-phosphate concentrations; phosphate starvation similarly induced the expression of PhoB-regulon genes *phoB* and *pstC* in wild-type and mutant cells (Fig. 1E). Thus, *ccna_03732* affects stalk synthesis independently of phosphate-mediated regulation. The defect in stalk elongation could also reflect a loss of cell polarity; however, the stalk-pole localization of DivJ-mCherry expressed from its native promoter was retained in the *ccna_03732*$^{A19T/G335N}$ strain (Fig. 1F).

Determining the enzymatic function of CCNA_03732

CCNA_03732 is annotated as a YihS-domain containing epimerase (GenBank ACL97197.3) and a BLAST search identified YihS as the closest *Escherichia coli* homologue (23). Exogenous expression of *E. coli* YihS in the *ccna_03732*$^{A19T/G335N}$ background did not complement the stalk defect (Fig. 2A) despite being expressed (Fig. 2B). YihS is part of a larger family of N-acyl-D-glucosamine 2-epimerases (AGEs) which isomerize a wide variety of carbohydrate substrates (24). *E. coli* encodes three additional AGE proteins (RffE, NanE, and ManA); therefore, we tested whether any of these genes could complement the CCNA_03732 mutation. Only expression of ManA was able to rescue stalk elongation (Fig. 2A); therefore, we will refer to CCNA_03732 as ManA. ManA is a phosphomannose isomerase (PMI) which catalyzes the interconversion of mannose 6-phosphate (M6P) and fructose 6-phosphate (F6P) (25). Although *E. coli* ManA expression does not fully recover stalk elongation when compared to wild-type (Fig. 2A), this may be because *E. coli* ManA is a type-I PMI (26) whereas *C. crescentus* ManA, based on its sequence homology to PMI from *Sinorhizobium meliloti*, appears

187 to be a type-III enzyme (27) (Fig. S1). Type I enzymes are zinc-dependent and specifically
188 catalyze M6P isomerization, whereas Type II PMIs are bifunctional and have guanosine
189 diphospho-D-mannose pyrophosphorylase activity (28). To date, the PMI from *S. meliloti* is the
190 only Type III enzyme and this protein has not been biochemically characterized. The three
191 subfamilies of PMIs have similar enzymatic functions but little sequence homology (26).
192 Alternatively, *E. coli* ManA may not fully complement in these experiments due to partial
193 inhibition of its activity by the C-terminal FLAG tag used to monitor protein expression.
194 To investigate the mechanism of the *ccna_03732*$^{A19T/G335N}$ (referred to as *manA**)
195 mutations, we performed a suppressor screen to isolate mutants which regained stalk elongation
196 (see Materials and Methods). This screen yielded a suppressor with a one-base deletion at the -
197 13-position relative to the transcription start site (Fig. 2C). We introduced a C-terminal mCherry
198 fusion at the native locus of *manA* in the wild-type, *manA**, and *manA**-suppressor strains to
199 assess protein expression and found that the suppressor mutation induced overexpression of
200 ManA* (Fig. 2D). Replacing the deleted cytosine in the suppressor mutant caused a reversion to
201 the short-stalk phenotype demonstrating the sufficiency of this SNP to rescue stalk elongation
202 (Fig. 2E). Since overexpression of ManA restored stalk synthesis, we concluded that the ManA*
203 mutant is a hypomorph with reduced enzymatic activity. Comparison of F6P/M6P ratios in wild-
204 type and *manA** strains demonstrated that wild-type cells maintained a 1:1 ratio in both high and
205 low phosphate whereas the ratio rises to 2:1 for *manA** cells in low phosphate (Fig. 2F). These
206 data suggest that in low phosphate, ManA* either cannot efficiently convert F6P to M6P or that
207 the mutation affects the preferred direction of isomerization. Mapping the A19T and G335N
208 mutations onto a homology model of ManA (produced using Phyre 2.0 (29) based on PDB
209 structure 1FP3 (30)) showed that the mutations are positioned near one another yet distant from

the predicted protein active site (Fig. 2G) (24) making it difficult to propose a mechanism for reduced ManA activity.

Effects of ManA* on bacterial envelope synthesis

Metabolic network maps (KEGG: amino sugar and nucleotide sugar metabolism) place ManA in a central position for regulating bacterial envelope synthesis (Fig. 3A) (31). F6P is a precursor for N-acetylglucosamine and N-acetylmuramic acid which are important metabolites for PG and core lipopolysaccharide (LPS) synthesis. M6P, which is metabolized to GDP-mannose, serves as a precursor for LPS O-antigen and exopolysaccharide (EPS) synthesis (32). Analysis of LPS demonstrated that the *manA** cells have approximately 83% less O-antigen-containing smooth-LPS relative to wild-type cells, while rough LPS (lacking O-antigen) was largely unaffected (Fig. 3B). A transposon insertion in *wbqP* (*ccna_01553*) inhibits O-antigen synthesis, likely by preventing the attachment of the first sugar (perosamine) to the undecaprenol carrier lipid, and is included as a negative control (33, 34); complementation of the transposon mutant by xylose-inducible expression of WbqP restored wild-type levels of O-antigen production. Comparison of the muropeptide content of PG from wild-type and *manA** cells did not reveal any gross changes in PG composition (Fig. 3C). Pulse-chase labeling of the PG with the fluorescent D-amino acid HADA (35) demonstrated the PG insertion was occurring at the base of the stalk in both wild-type and *manA** cells (Fig. 3D). Lastly, production of EPS was assessed by the presence of a mucoid phenotype when grown on agar plates supplemented with 3% sucrose; wild-type cells producing EPS were mucoid while *manA** cells were dull in appearance (Fig. 3E). Non-EPS producing strains (CB15 and NA1000 ΔMGE (mobile-genetic element)) were included as controls (32). Together, these findings showed that F6P-dependent

metabolism was unaffected in the *manA** strain, whereas M6P-dependent processes were inhibited. This is consistent with the ManA* mutant being an enzymatic hypomorph leading to an increased F6P:M6P ratio (Fig. 2D, F). To determine whether these changes in cellular envelope were the cause of the stalk elongation defect, stalk lengths were measured in NA1000 strains lacking either EPS (ΔMGE) or O-antigen (Tn5::*wbqP* (33, 34)) (Fig. 3F). Inhibition of EPS production had no significant effect on stalk length; however, O-antigen disruption reduced stalk length although not to the same degree as the *manA** strain (Fig. 3F). Inducible expression of WbqP was sufficient to complement the Tn5::*wbqP* phenotype (Fig. 3F). While the partial effect of Tn5::*wbqP* on stalk length suggests that O-antigen synthesis plays a role in stalk elongation, an alternative explanation is that the inhibition of this pathway alters the flux through connected metabolic pathways leading to stalk elongation defects.

ManA regulates entry into stationary phase

Since F6P and M6P feed into a variety of metabolic pathways, we performed metabolomic analyses of wild-type and *manA** cells grown in low-phosphate to assess global changes in cellular metabolism. As expected, wild-type cells had higher levels of M6P as compared to *manA** cells; additionally, we found higher levels of TCA cycle intermediates in wild-type cells (Fig. 4A). Accumulation of TCA cycle intermediates is consistent with bacteria entering stationary phase (36, 37), therefore, we performed long term growth curves to assess stationary phase entry. When cultured in HIGG- 30 μM phosphate, wild-type growth plateaued at OD_{660}=1.8; by contrast, *manA** cells continued to divide to OD_{660}=2.5, suggesting that they failed to enter stationary phase (Fig. 4B). Imaging of the cells at 72 h confirms that the increased OD is due to cell growth as opposed to filamentation or other changes in cell morphology (Fig.

4C). As observed with regards to stalk elongation, exogenous expression of ManA in the mutant background restored wild-type growth kinetics (Fig. 4B). Consistent with their increased proliferation, *manA** cells had lower expression of known stationary-phase genes *cspD*, *katG*, and *spdR* (38) following 48 h of culture in low-phosphate media (Fig. 4D) and deletion of the stationary-phase response regulator *spdR* inhibited stalk elongation (Fig. 4E).

Stationary-phase entry and the stringent response are, in part, regulated by the production of the alarmone guanosine 3',5'-bispyrophosphate (ppGpp) (39, 40). Overexpression of the N-terminal domain of the ppGpp synthetase RelA results in the constitutive production of ppGpp and decreased growth rate in *E. coli* (41). To test whether stationary phase entry was necessary for stalk elongation in *C. crescentus*, we overexpressed truncated RelA in the *manA** cells; overproduction of ppGpp resulted in a significant increase in stalk length (Fig. 4F).

Discussion

C. crescentus stalks elongate under phosphate-limited conditions, however the mechanism is not well understood. Perturbation of genes associated with peptidoglycan synthesis results in shorter stalks (7, 8, 15); however, this system appears to be highly redundant as even the deletion of multiple PBPs does not abrogate stalk synthesis completely. Recently, a fluorescent fusion to the cytoskeletal protein MreB was shown to be functional with regards to cell growth, but this fusion did not localize at the poles nor support stalk formation (9), suggesting that the GFP-tag interferes with protein-protein interactions necessary for stalk synthesis.

To identify novel regulatory mechanisms of stalk elongation, we used chemical mutagenesis to introduce single-nucleotide polymorphisms (SNPs) and isolated mutants with stalk elongation defects. One particular strain had two SNPs in *ccna_03732* (*manA*), a phosphomannose isomerase (Fig. 2A), both of which were required for a stalk-deficient phenotype (Fig. 1A-D). The SNPs were on the protein surface in close proximity to one another, yet quite distant from the enzyme active site (Fig 2G). This suggests that these residues may mediate a protein-protein interaction. Although we could not find any report of PMI enzymes oligomerizing, other AGE family members can form dimers (42, 43). These SNPs affected the relative levels of F6P and M6P (Fig. 2F) and cellular envelope biosynthesis (Fig. 3A-E), but not the transcriptional response to phosphate limitation (Fig. 1E). These findings demonstrate that cellular metabolism regulates stalk elongation independently of phosphate starvation.

Disruption of sugar-phosphate metabolism results in cell shape phenotypes in a wide range of organisms. In *Bacillus subtilis*, deletion of *manA* leads to cells with an elongated spheroid morphology (44). This morphology is due, in part, to a decrease in wall techoic acid

(WTA) production which affects cell wall architecture (44). PMI plays a role in eukaryotic cell shape as well. Deletion of PMI in the fungus *Aspergillus fumigatus* affects conidiation and produces a thickened chitin-rich cell wall (45), while in the protozoan *Leishmania mexicana,* Δ*pmi* promastigotes were shorter and rounder than wild-type (46).

While *manA* disruption affects cell shape in both *C. crescentus* and *B. subtilis*, it appears that the mechanisms may be quite different. In Gram-positive *B. subtilis*, ManA specifically reduces the levels of the cell wall carbohydrates glucose and N-acetylgalactosamine (GalNAc) without affecting N-acetylglucosamine (GlcNAc). Thus, Δ*manA* affects WTA but not PG synthesis. By contrast, Gram-negative *C. crescentus* does not produce WTA, and the composition of the PG was not affected in the *manA** strain (Fig. 3C); thus, another mechanism is required to explain the stalk elongation phenotype. While the *manA** mutations affected LPS O-antigen and EPS production, these envelope perturbations were not solely responsible for the mutant cell defect (Fig. 3F).

In addition to interfering with cellular envelope biosynthesis, the metabolic imbalance produced by the *manA** mutations prevents stationary-phase entry of *C. crescentus* (Fig. 4A-D). The accumulation of sugar-phosphates triggers a variety of bacterial stress responses. In *B. subtilis*, a build-up of M6P leads to increased expression of the stress sigma factors σ^{X} and σ^{W} (47) as well as derepression of the *glcR-phoC* operon (48). In *E. coli*, elevated concentrations of sugar-phosphates leads to growth inhibition (49), induction of the stringent response (50), and expression of the stress-response gene *uspA* (51). This response is mediated, in part, by the small RNA *sgrS* which directs the degradation of mRNAs important for sugar-phosphate transport including *ptsG* and *manXYZ* as well as the stabilization of the phosphatase *yigL* (52-54). Interestingly, while alterations to sugar-phosphate homeostasis promote the stringent response

314 and growth arrest in *B. subtilis* and *E. coli*, F6P accumulation in *C. crescentus* due to the *manA**
315 mutations prevents stationary-phase entry. *C. crescentus* does not encode homologues of SgrRS,
316 UspA, or GlcR; therefore, further investigations will be required to identify the sensor and
317 downstream targets of sugar-phosphate stress in *C. crescentus*.
318

Materials and Methods

Bacterial strains, plasmids, and growth conditions

The strains, plasmids, and primers used in this study are described in Supplemental Tables S1, S2, and S3, respectively. Details regarding strain construction are available in the Supplementary Methods.

C. crescentus wild-type strains NA1000, CB15, and their derivatives were grown at 30 °C in peptone-yeast-extract (PYE) medium (55) for routine culturing. To regulate phosphate levels, *C. crescentus* was grown in Hutner-Imidazole-Glucose-Glutamate (HIGG) media with varying concentrations of phosphate (1-1000 μM) (19). *E. coli* strains were grown at 37 °C in LB medium. When necessary, antibiotics were added at the following concentrations: kanamycin 30 μg ml^{-1} in broth and 50 μg ml^{-1} in agar (abbreviated 30:50) for *E. coli* and 5:25 for *C. crescentus*; tetracycline 12:12 *E. coli* and 1:2 *C. crescentus*. Gene expression was induced in *C. crescentus* with 0.003-0.3% (w/v) xylose. Growth curves were determined by measuring OD (660 nm) at the indicated time points.

Chemical mutagenesis and screening for stalk-elongation mutants

C. crescentus NA1000 cells (1 mL) were grown in HIGG-1 mM phosphate overnight and treated with 200 μg mL^{-1} 1-methyl-3-nitro-1-nitrosoguanidine (NTG, TCI America) for 50 min at 30 °C to induce DNA mutations. The cells were washed once in HIGG without phosphate and resuspended in 100 mL HIGG- 1 μM phosphate to promote stalk elongation. After 72 h, cells were pelleted at 16,000 x g for 20 min, resuspended in 5.5 mL of HIGG- 1 μM phosphate, and

342 mixed 1:1 with Percoll (GE Healthcare) to establish a density gradient. This mixture was
343 centrifuged for 1 h at 9,500 x g and cells from the bottom of the tube were recovered using a
344 Pasteur pipette. After two additional Percoll gradients, the bottom cells were plated on PYE
345 plates to isolate individual mutants. 384 individual colonies were grown in HIGG- 1 μM
346 phosphate and visually screened for stalk defects.
347
348 Whole-genome sequencing
349 Genomic DNA was isolated from NA1000 and SDM1, barcoded sequencing libraries were
350 constructed using the NEBNext Fast DNA Fragmentation & Library Prep Set for Ion Torrent
351 (New England Biolabs), and templated using the Ion PI Hi-Q Chef kit (Thermo Fisher). The
352 libraries were sequenced on an Ion Proton system (Thermo Fisher) (NA1000: 2,148,749 reads,
353 mean read length=132 bp, mean sequencing depth=70X; SDM1: 1,976,601 reads, mean read
354 length=132 bp, mean sequencing depth=64X). Reads were mapped to the NA1000 genomic
355 sequence (NCBI NC_011916.1) and variants were called using Ion Reporter software (Thermo
356 Fisher). SNPs present in both SDM1 and our lab strain of NA1000 were eliminated from
357 analysis.
358
359 Cosmid conjugation
360 *E. coli* cosmid-library strains (kindly provided by Lucy Shapiro, Stanford University) (20) and
361 SDM1 *C. crescentus* cells were grown overnight in LB and PYE, respectively. 100 μL of each
362 cosmid-strain was mixed with 900 μL SDM1, centrifuged at 8,000 x *g* for 2 min, washed once in
363 PYE, and the final pellet was resuspended in 20 μL PYE. The mixed and concentrated samples
364 were dropped onto PYE plates and incubated at 30 °C for 6 h. Samples of the bacterial

conjugants were streaked onto PYE plates containing 25 μg mL^{-1} kanamycin and 30 μg mL^{-1} nalidixic acid; *C. crescentus* cells are naturally resistant to nalidixic acid allowing for selection of *C. crescentus* cells that have received the cosmid.

*manA** suppressor screen

A single colony of the *manA** strain grown 2 mL of HIGG- 1mM phosphate overnight at 30°C. 1 mL of the culture was washed twice in HIGG (without phosphate), resuspended in HIGG- 1μM phosphate, and grown for 2 days at 30°C. The culture was centrifuged at 10,000 x g for 10 min. The supernatant containing buoyant potential suppressor cells was collected and centrifuged at 28,000 x g for 30 min. The pelleted cells were then resuspended in 20mL of HIGG- 1μM phosphate. This purification process was repeated every 48 h; after two weeks the culture was streaked onto PYE plates to isolate individual colonies. Colonies were subsequently grown in HIGG- 1μM phosphate and screened by microscopy for stalk recovery.

Microscopy and image analysis

Cells were spotted onto 1% agarose pads made in the corresponding growth medium. Microscopy was performed on a Nikon TiE inverted microscope equipped with a Prior Lumen 220PRO illumination system, Zyla sCMOS 5.5-megapixel camera, CFI Plan Apochromat 100X oil immersion objective (NA 1.45, WD 0.13 mm), and NIS Elements software for image acquisition. Stalk lengths were measured using ImageJ v. 1.48q (NIH).

388 Quantitative RT-PCR (qRT-PCR)

389 RNA was extracted from bacterial cultures using the Qiagen RNeasy kit. Following DNase
390 digestion, RNA (5 ng μl^{-1}) was reverse transcribed using the High Capacity cDNA Reverse
391 Transcription Kit (Applied Biosystems). 1 µl of cDNA was used as a template in a 10 µl qRT-
392 PCR reaction performed with Power SYBR reagent (Applied Biosystems). qRT-PCR was
393 performed on an ABI QuantStudio 6 using the ΔΔCt method. *rpoD* or *rpoH* expression was used
394 as the loading control as indicated.

395

396 Western blot analysis

397 *C. crescentus* cells were grown overnight in the indicated medium and cell concentration was
398 normalized by OD_{660}. 1 mL samples of OD_{660}=0.5 were collected by centrifugation (8,000 x *g*, 2
399 min), resuspended in 100 µL 1X Laemmli buffer, and boiled for 5 min to denature proteins.
400 Protein samples were separated on 10% SDS-PAGE gels, transferred to PVDF membrane, and
401 probed using the following antibodies: FLAG (1:500, sc-166355, Santa Cruz) and DivK (1:1000,
402 kind gift from Lucy Shapiro, Stanford University (56)).

403

404 Metabolomics

405 *C. crescentus* cells were grown overnight in HIGG- 1 mM phosphate, back diluted, and grown to
406 OD_{660}=0.3. For high-phosphate samples, 5 mL of OD_{660}=0.3 was filtered onto a 0.2 µm pore-size
407 nylon membrane (Millipore GNWP04700). For low-phosphate samples, 5 mL of OD_{660}=0.3 was
408 washed twice in HIGG lacking phosphate, resuspended in 5 mL HIGG- 1 µM phosphate, grown
409 for 6 h, and then filtered onto nylon membranes. The filters were immediately quenched in 1.2
410 mL ice-cold 40:40:20 acetonitrile:methanol:water containing 0.5% (v/v) formic acid. The

411 samples were incubated at -20 °C for 15 min and the solutions were transferred to pre-chilled 2
412 mL microcentrifuge tubes containing 50 mg 0.1 mm glass beads (Med Supply Partners, NA-
413 GB01-RNA). The solvent was neutralized by adding 100 µL 1.9M ammonium carbonate and
414 cells were lysed on a Qiagen TissueLyser for 5 min at 30 Hz. Samples were centrifuged at
415 16,000 x *g* for 10 min at 4 °C to pellet unbroken cells and the supernatant was transferred to a
416 pre-chilled microcentrifuge tube and frozen on dry ice. Samples were sent to the Metabolomics
417 Core Facility of the Cancer Institute of New Jersey (New Brunswick, NJ) for analysis by liquid
418 chromatography/mass-spectrometry (LC/MS) as previously described (57). Briefly, metabolites
419 were analyzed on a Q Exactive PLUS hybrid quadrupole-orbitrap mass spectrometer
420 (ThermoFisher Scientific) coupled to hydrophilic interaction chromatography (HILIC).
421 Chromatography was performed on an UltiMate 3000 UHPLC system with an XBridge BEH
422 Amide column (150 mm × 2.1 mm, 2.5 µM particle size, Waters). The LC solvents were: A
423 (95%:5% H2O:acetonitrile with 20mM ammonium acetate, 20mM ammonium hydroxide, pH
424 9.4) and B (20%:80% H2O:acetonitrile with 20 mM ammonium acetate, 20 mM ammonium
425 hydroxide, pH 9.4). The gradient was 0 min, 100% B; 3 min, 100% B; 3.2 min, 90% B; 6.2 min,
426 90% B; 6.5 min, 80% B; 10.5 min, 80% B; 10.7 min, 70% B; 13.5 min, 70% B; 13.7 min, 45%
427 B; 16 min, 45% B; 16.5 min, 100% B. The flow rate was 300 µl min^{-1}. Injection volume was 5 µl
428 and column temperature 25°C. The MS scans were in negative ion mode with a resolution of
429 70,000 at m/z 200 and the scan range was 75−1000. Since F6P and glucose 1-phosphate have the
430 same molecular weight and co-elute by LC, it is impossible to distinguish between these two
431 sugar-phosphates. To enable quantification of F6P, we replaced the glucose in our standard
432 HIGG media with deuterated 2-D glucose (Cambridge Isotope Laboratories, DLM-1271). During

433 the isomerization of glucose to fructose, the deuterium at C-2 is replaced with hydrogen, leading
434 to a 1 mass-unit shift between these sugars and enabling their distinction by MS.
435
436 Lipopolysaccharide (LPS) purification and analysis
437 LPS was purified essentially as previously described (34, 58). Briefly, 5 ml of *C. crescentus* cells
438 grown in HIGG- 1 µM phosphate (OD_{660} = 0.5) were collected and washed once in 10 mM
439 HEPES, pH 7.2. Cells were resuspended in 250 µl TE buffer (10 mM Tris, 1 mM EDTA, pH
440 7.2) and frozen overnight at -20 °C. Cells were thawed, treated with 1 µl DNase (0.5 mg ml^{-1}),
441 20 µl lysozyme (10 mg ml^{-1}), and 3 µl $MgCl_2$ (1 M), and incubated at room temperature for 15
442 min. For each sample, 36.25 µl was mixed with 12.5 µl 4X SDS-sample buffer and boiled at 100
443 °C for 10 min. After cooling to room temperature, 1.25 µl proteinase K (20 mg ml^{-1}) was added
444 and samples were incubated at 60 °C for 1 h. LPS samples were resolved by Tris-Tricine SDS-
445 PAGE on a 16% acrylamide gel containing 3% crosslinker followed by staining with the Pro-Q
446 Emerald 300 LPS stain kit according to the manufacturer's protocol (Thermo Scientific). Images
447 were acquired on a Bio-Rad ChemiDoc MP using UV excitation and a 530 nm emission filter
448 and band intensities were quantified using Image Lab (Bio-Rad).
449
450 Peptidoglycan (PG) purification and analysis
451 *C. crescentus* cells (500 mL) were grown in HIGG- 1 µM phosphate. Peptidoglycan
452 muropeptides were purified from *C. crescentus* as previously described (59) and separated on a
453 reversed-phase C18 column (Thermo Scientific; 250 x 4.6-mm column, 3-µm particle size) held
454 at 55 °C. The LC solvent system consisted of 50 mM sodium phosphate [pH 4.35] with 0.4%
455 sodium azide (solvent A) and 75 mM sodium phosphate, pH 4.95 + 15% (v/v) methanol (solvent

B). The solvent flow rate was 0.5 mL min^{-1} and a linear gradient to 100% solvent B was performed over 135 min. Muropeptide elution was monitored at 205 nm.

Pulse-chase fluorescent labeling of PG

Cells were grown in HIGG- 1 μM phosphate for 48 h prior to labeling. Aliquots of each culture (250 μL) were labeled with 0.25 mM HADA (35), a fluorescent D-amino acid analog, for 30 min at 30 °C. The cells were washed 3 times in PBS and imaged using DAPI excitation/emission filters.

Exopolysaccharide (EPS) production assay

Strains were streaked onto HIGG- 1 μM phosphate agar plates supplemented with 3% (w/v) sucrose. EPS production was determined by assessing mucoidy. CB15 and NA1000 ΔMGE were used as non-EPS producing controls (32).

Acknowledgements

We thank Lucy Shapiro (Stanford University) and Christine Jacobs-Wagner (Yale University) for providing reagents and Xiaoyang Su and the metabolomics core facility at the Cancer Institute of New Jersey for their experimental assistance. Funding was provided by National Science Foundation CAREER Award MCB-1553004 to E.A.K.

Author contributions

K.dY., G.S., and E.A.K. designed, performed, and analyzed experiments. E.A.K. wrote the manuscript. K.dY. and G.S. edited the manuscript.

References

1. Stove Poindexter JL, Cohen-Bazire G. 1964. The fine structure of stalked bacteria belonging to the family Caulobacteraceae. Journal of Cell Biology 23:587-607.
2. Tsang PH, Li G, Brun YV, Freund LB, Tang JX. 2006. Adhesion of single bacterial cells in the micronewton range. PNAS 103:5764-5768.
3. Gonin M, Quardokus EM, O'Donnol D, Maddock J, Brun YV. 2000. Regulation of stalk elongation by phosphate in *Caulobacter crescentus*. J Bacteriol 182:337-347.
4. Ireland MM, Karty JA, Quardokus EM, Reilly JP, Brun YV. 2002. Proteomic analysis of the *Caulobacter crescentus* stalk indicates competence for nutrient uptake. Mol Microbiol 45:1029-41.
5. Wagner JK, Setayeshgar S, Sharon LA, Reilly JP, Brun YV. 2006. A nutrient uptake role for bacterial cell envelope extensions. Proc Natl Acad Sci U S A 103:11772-7.
6. Klein EA, Schlimpert S, Hughes V, Brun YV, Thanbichler M, Gitai Z. 2013. Physiological role of stalk lengthening in *Caulobacter crescentus*. Commun Integr Biol 6:e24561.
7. Strobel W, Moll A, Kiekebusch D, Klein KE, Thanbichler M. 2014. Function and localization dynamics of bifunctional penicillin-binding proteins in *Caulobacter crescentus*. J Bacteriol 196:1627-39.
8. Yakhnina AA, Gitai Z. 2013. Diverse functions for six glycosyltransferases in *Caulobacter crescentus* cell wall assembly. J Bacteriol 195:4527-35.

9. Billini M, Biboy J, Kuhn J, Vollmer W, Thanbichler M. 2019. A specialized MreB-dependent cell wall biosynthetic complex mediates the formation of stalk-specific peptidoglycan in *Caulobacter crescentus*. PLoS Genet 15:e1007897.
10. Seitz LC, Brun YV. 1998. Genetic analysis of mecillinam-resistant mutants of *Caulobacter crescentus* deficient in stalk biosynthesis. J Bacteriol 180:5235-9.
11. Wagner JK, Galvani CD, Brun YV. 2005. *Caulobacter crescentus* requires RodA and MreB for stalk synthesis and prevention of ectopic pole formation. J Bacteriol 187:544-53.
12. Lee TK, Tropini C, Hsin J, Desmarais SM, Ursell TS, Gong E, Gitai Z, Monds RD, Huang KC. 2014. A dynamically assembled cell wall synthesis machinery buffers cell growth. Proc Natl Acad Sci U S A 111:4554-9.
13. Rohs PDA, Buss J, Sim SI, Squyres GR, Srisuknimit V, Smith M, Cho H, Sjodt M, Kruse AC, Garner EC, Walker S, Kahne DE, Bernhardt TG. 2018. A central role for PBP2 in the activation of peptidoglycan polymerization by the bacterial cell elongation machinery. PLoS Genet 14:e1007726.
14. Stankeviciute G, Miguel AV, Radkov A, Chou S, Huang KC, Klein EA. 2019. Differential modes of crosslinking establish spatially distinct regions of peptidoglycan in *Caulobacter crescentus*. Mol Microbiol 111:995-1008.
15. Kuhn J, Briegel A, Morschel E, Kahnt J, Leser K, Wick S, Jensen GJ, Thanbichler M. 2010. Bactofilins, a ubiquitous class of cytoskeletal proteins mediating polar localization of a cell wall synthase in *Caulobacter crescentus*. EMBO J 29:327-39.
16. Hughes HV, Huitema E, Pritchard S, Keiler KC, Brun YV, Viollier PH. 2010. Protein localization and dynamics within a bacterial organelle. PNAS 107:5599-604.

17. Ryan KR, Taylor JA, Bowers LM. 2010. The BAM complex subunit BamE (SmpA) is required for membrane integrity, stalk growth and normal levels of outer membrane beta-barrel proteins in *Caulobacter crescentus*. Microbiology 156:742-56.
18. Poggio S, Takacs CN, Vollmer W, Jacobs-Wagner C. 2010. A protein critical for cell constriction in the Gram-negative bacterium *Caulobacter crescentus* localizes at the division site through its peptidoglycan-binding LysM domains. Mol Microbiol 77:74-89.
19. Poindexter JS. 1978. Selection for nonbuoyant morphological mutants of *Caulobacter crescentus*. J Bacteriol 135:1141-5.
20. Alley MR, Gomes SL, Alexander W, Shapiro L. 1991. Genetic analysis of a temporally transcribed chemotaxis gene cluster in *Caulobacter crescentus*. Genetics 129:333-41.
21. Caspi R, Billington R, Fulcher CA, Keseler IM, Kothari A, Krummenacker M, Latendresse M, Midford PE, Ong Q, Ong WK, Paley S, Subhraveti P, Karp PD. 2017. The MetaCyc database of metabolic pathways and enzymes. Nucleic Acids Res doi:4559117 [pii]

10.1093/nar/gkx935.
22. Christen B, Abeliuk E, Collier JM, Kalogeraki VS, Passarelli B, Coller JA, Fero MJ, McAdams HH, Shapiro L. 2011. The essential genome of a bacterium. Mol Syst Biol 7:1-7.
23. Altschul SF, Gish W, Miller W, Myers EW, Lipman DJ. 1990. Basic local alignment search tool. J Mol Biol 215:403-10.
24. Itoh T, Mikami B, Hashimoto W, Murata K. 2008. Crystal structure of YihS in complex with D-mannose: structural annotation of *Escherichia coli* and *Salmonella enterica yihS*-encoded proteins to an aldose-ketose isomerase. J Mol Biol 377:1443-59.

25. Gao H, Yu Y, Leary JA. 2005. Mechanism and kinetics of metalloenzyme phosphomannose isomerase: measurement of dissociation constants and effect of zinc binding using ESI-FTICR mass spectrometry. Anal Chem 77:5596-603.
26. Proudfoot AE, Turcatti G, Wells TN, Payton MA, Smith DJ. 1994. Purification, cDNA cloning and heterologous expression of human phosphomannose isomerase. Eur J Biochem 219:415-23.
27. Schmidt M, Arnold W, Niemann A, Kleickmann A, Puhler A. 1992. The *Rhizobium meliloti pmi* gene encodes a new type of phosphomannose isomerase. Gene 122:35-43.
28. Jensen SO, Reeves PR. 1998. Domain organisation in phosphomannose isomerases (types I and II). Biochim Biophys Acta 1382:5-7.
29. Kelley LA, Mezulis S, Yates CM, Wass MN, Sternberg MJ. 2015. The Phyre2 web portal for protein modeling, prediction and analysis. Nat Protoc 10:845-58.
30. Itoh T, Mikami B, Maru I, Ohta Y, Hashimoto W, Murata K. 2000. Crystal structure of N-acyl-D-glucosamine 2-epimerase from porcine kidney at 2.0 A resolution. J Mol Biol 303:733-44.
31. Kanehisa M, Goto S. 2000. KEGG: Kyoto encyclopedia of genes and genomes. Nucleic Acids Res 28:27-30.
32. Herr KL, Carey AM, Heckman TI, Chavez JL, Johnson CN, Harvey E, Gamroth WA, Wulfing BS, Van Kessel RA, Marks ME. 2018. Exopolysaccharide production in *Caulobacter crescentus*: A resource allocation trade-off between protection and proliferation. PLoS One 13:e0190371.

33. Awram P, Smit J. 2001. Identification of lipopolysaccharide O antigen synthesis genes required for attachment of the S-layer of *Caulobacter crescentus*. Microbiology 147:1451-60.
34. Cabeen MT, Murolo MA, Briegel A, Bui NK, Vollmer W, Ausmees N, Jensen GJ, Jacobs-Wagner C. 2010. Mutations in the lipopolysaccharide biosynthesis pathway interfere with crescentin-mediated cell curvature in *Caulobacter crescentus*. J Bacteriol 192:3368-78.
35. Kuru E, Hughes HV, Brown PJ, Hall E, Tekkam S, Cava F, de Pedro MA, Brun YV, VanNieuwenhze MS. 2012. In situ probing of newly synthesized peptidoglycan in live bacteria with fluorescent D-amino acids. Angew Chem Int Ed Engl 51:12519-23.
36. Chang DE, Conway T. 2005. Metabolic genomics. Adv Microb Physiol 50:1-39.
37. Jozefczuk S, Klie S, Catchpole G, Szymanski J, Cuadros-Inostroza A, Steinhauser D, Selbig J, Willmitzer L. 2010. Metabolomic and transcriptomic stress response of *Escherichia coli*. Mol Syst Biol 6:364.
38. da Silva CA, Lourenco RF, Mazzon RR, Ribeiro RA, Marques MV. 2016. Transcriptomic analysis of the stationary phase response regulator SpdR in *Caulobacter crescentus*. BMC Microbiol 16:66.
39. Hirsch M, Elliott T. 2002. Role of ppGpp in rpoS stationary-phase regulation in *Escherichia coli*. J Bacteriol 184:5077-87.
40. Traxler MF, Summers SM, Nguyen HT, Zacharia VM, Hightower GA, Smith JT, Conway T. 2008. The global, ppGpp-mediated stringent response to amino acid starvation in *Escherichia coli*. Mol Microbiol 68:1128-48.

589 41. Zhu M, Dai X. 2019. Growth suppression by altered (p)ppGpp levels results from non-
590 optimal resource allocation in *Escherichia coli*. Nucleic Acids Res
591 doi:10.1093/nar/gkz211.
592 42. Halsor MJH, Rothweiler U, Altermark B, Raeder ILU. 2019. The crystal structure of the
593 N-acetylglucosamine 2-epimerase from Nostoc sp. KVJ10 reveals the true dimer. Acta
594 Crystallogr D Struct Biol 75:90-100.
595 43. Kasumi T, Mori S, Kaneko S, Matsumoto H, Kobayashi Y, Koyama Y. 2014.
596 Characterization of mannose isomerase from a cellulolytic Actinobacteria *Thermobifida*
597 *fusca* MBL10003. Journal of Applied Glycoscience 61:21-25.
598 44. Elbaz M, Ben-Yehuda S. 2010. The metabolic enzyme ManA reveals a link between cell
599 wall integrity and chromosome morphology. PLoS Genet 6:e1001119.
600 45. Fang W, Yu X, Wang B, Zhou H, Ouyang H, Ming J, Jin C. 2009. Characterization of the
601 *Aspergillus fumigatus* phosphomannose isomerase Pmi1 and its impact on cell wall
602 synthesis and morphogenesis. Microbiology 155:3281-93.
603 46. Garami A, Ilg T. 2001. The role of phosphomannose isomerase in *Leishmania mexicana*
604 glycoconjugate synthesis and virulence. J Biol Chem 276:6566-75.
605 47. Turner MS, Helmann JD. 2000. Mutations in multidrug efflux homologs, sugar
606 isomerases, and antimicrobial biosynthesis genes differentially elevate activity of the
607 sigma(X) and sigma(W) factors in *Bacillus subtilis*. J Bacteriol 182:5202-10.
608 48. Morabbi Heravi K, Manzoor I, Watzlawick H, de Jong A, Kuipers OP, Altenbuchner J.
609 2019. Phosphosugar stress in *Bacillus subtilis*: intracellular accumulation of mannose 6-
610 phosphate derepressed the *glcR-phoC* operon from repression by GlcR. J Bacteriol 201.

611 49. Kadner RJ, Murphy GP, Stephens CM. 1992. Two mechanisms for growth inhibition by
612 elevated transport of sugar phosphates in *Escherichia coli*. J Gen Microbiol 138:2007-14.
613 50. Kessler JR, Cobe BL, Richards GR. 2017. Stringent response regulators contribute to
614 recovery from glucose phosphate stress in *Escherichia coli*. Appl Environ Microbiol 83.
615 51. Persson O, Valadi A, Nystrom T, Farewell A. 2007. Metabolic control of the *Escherichia*
616 *coli* universal stress protein response through fructose-6-phosphate. Mol Microbiol
617 65:968-78.
618 52. Papenfort K, Sun Y, Miyakoshi M, Vanderpool CK, Vogel J. 2013. Small RNA-mediated
619 activation of sugar phosphatase mRNA regulates glucose homeostasis. Cell 153:426-37.
620 53. Rice JB, Vanderpool CK. 2011. The small RNA SgrS controls sugar-phosphate
621 accumulation by regulating multiple PTS genes. Nucleic Acids Res 39:3806-19.
622 54. Vanderpool CK, Gottesman S. 2004. Involvement of a novel transcriptional activator and
623 small RNA in post-transcriptional regulation of the glucose phosphoenolpyruvate
624 phosphotransferase system. Mol Microbiol 54:1076-89.
625 55. Poindexter JS. 1964. Biological properties and classification of the *Caulobacter* group.
626 Bacteriol Rev 28:231-95.
627 56. Jacobs C, Hung D, Shapiro L. 2001. Dynamic localization of a cytoplasmic signal
628 transduction response regulator controls morphogenesis during the *Caulobacter* cell
629 cycle. Proc Natl Acad Sci U S A 98:4095-100.
630 57. Poillet-Perez L, Xie X, Zhan L, Yang Y, Sharp DW, Hu ZS, Su X, Maganti A, Jiang C,
631 Lu W, Zheng H, Bosenberg MW, Mehnert JM, Guo JY, Lattime E, Rabinowitz JD,
632 White E. 2018. Autophagy maintains tumour growth through circulating arginine. Nature
633 563:569-573.

58. Stankeviciute G, Guan Z, Goldfine H, Klein EA. 2019. *Caulobacter crescentus* adapts to phosphate starvation by synthesizing anionic glycoglycerolipids and a novel glycosphingolipid. MBio 10:e00107-19.

59. Desmarais SM, Cava F, de Pedro MA, Huang KC. 2014. Isolation and preparation of bacterial cell walls for compositional analysis by ultra performance liquid chromatography. J Vis Exp 83:e51183.

642 **Figure legends**

643

644 **Figure 1. Isolation and mapping of a stalk-deficient mutant.** (A) Screening a library of
645 chemically-mutagenized *C. crescentus* strains identified Stalk Deficient Mutant 1 (SDM1;
646 KD80). This mutant phenotype was rescued by complementation with two individual cosmids
647 containing 20-30 kb genomic fragments (KD9, KD10). Scale bar: 5 μm. (B) A diagram of the
648 two complementing cosmids shows their region of overlap. Within the overlapping genes, only
649 *ccna_03732* has SNPs (denoted by *) as determined by whole-genome sequencing. (C-D) The
650 SDM1 stalk phenotype was complemented by xylose-inducible expression of wild-type
651 *ccna_03732* (KD64). Introduction of both *ccna_03732* SNPs into NA1000 was sufficient to
652 produce the stalk-elongation defect (KD145), whereas each individual SNP had either no effect
653 (A19T; KD174) or a partial effect (G335N; KD175). Scale bar: 5 μm. Stalk lengths were
654 measured using ImageJ (error bars are SEM, ANOVA $F(3,196)=76.8$, $P<0.0001$; * post-hoc
655 comparisons using Bonferroni test, $P<0.05$). (E) Wild-type and *ccna_03732*$^{A19T/G335N}$ cells were
656 grown for 24 h in HIGG-1 mM phosphate. For low phosphate samples, cells were washed twice
657 in HIGG without phosphate, resuspended in HIGG without phosphate and grown for an
658 additional 6 h. Total RNA was collected from each sample for qRT-PCR analysis of the PhoB-
659 regulated genes *phoB* and *pstC*. Gene expression was normalized to *rpoD* and sample
660 expressions were normalized to wild-type 1 mM phosphate (error bars are SEM, n=3). Strong
661 induction of both genes confirmed that the *ccna_03732* SNPs do not affect the sensing of
662 phosphate starvation. (F) Wild-type and *ccna_03732*$^{A19T/G335N}$ cells expressing DivJ-mCherry
663 from its native locus (KD GB212, EK394) were grown for 48 h in HIGG- 1 μM phosphate prior
664 to imaging. Scale bar: 5 μm.

Figure 2. CCNA_03732 is a phosphomannose isomerase. (A) Exogenous expression of the closest *E. coli* homologue to CCNA_03732, YihS, did not complement the stalk elongation defect (KD153). Screening the other AGE-family isomerases (EK266, EK268, EK270) demonstrated that only ManA can rescue stalk synthesis in the *ccna_03732*$^{A19T/G335N}$ strain. (B) Western blot analysis of FLAG-tagged CCNA_03732 and YihS (both wild-type and codon-optimized) showed that they are expressed at comparable levels. Therefore, the inability of YihS to rescue stalk-elongation is a reflection of differing enzymatic activities rather than expression level. (C) Sequencing of the *manA* locus in the suppressor strain identified a single base deletion upstream of the *manA* transcription start site. (D) Native-locus mCherry fusions to ManA showed that the stalk elongation phenotype can be suppressed by dramatic overexpression of ManA* (KD160, KD161, KD162). Images were acquired with the same exposure time and the lookup tables (LUTs) were adjusted identically for each sample. Scale bar: 5 μm. (E) Reinsertion of the deleted base into the suppressor strain reverted the stalk deficiency phenotype (KD170, KD186). Scale bar: 5 μm. (F) Metabolomic analysis of F6P and M6P levels showed that wild-type cells maintain a 1:1 ratio in both low and high phosphate, whereas *manA** (KD145) cells increase their relative levels of F6P as phosphate decreases (error bars are SEM, n=3; * p=0.04, one-tailed *t*-test). (G) A cartoon of the ManA protein identifies the locations of the ManA* SNPs (red triangles) as well as the predicted active site residues (yellow triangles). The active site residues are based on an alignment to the AGE protein YihS (Fig. S1) (24). A homology model of ManA (based on PDB 1FP3) shows that the ManA mutations (red) are near one another but not near the enzyme active site (yellow).

Figure 3. ManA* results in alterations to specific cellular envelope components. (A) ManA regulates the interconversion of F6P and M6P. These metabolites are important precursors for the synthesis of cellular envelope components including LPS, PG, and EPS. (B) LPS was extracted from wild-type, *manA** (KD145), Tn5::*wbqP* (CJW1249), and Tn5::*wbqP*/P_{xyl}-*wbqP* (EK393) cells grown for 48 h in HIGG- 1 μM phosphate with 0.03% xylose and separated by Tris-Tricine SDS-PAGE. (C) Comparisons of muropeptides from wild-type and *manA** cells grown in HIGG- 1 μM phosphate did not yield any gross changes in PG composition. (D) Wild-type and *manA** cells were grown in HIGG-1 μM phosphate for 48 h prior to pulse-chase labeling with HADA for 30 min to label regions of active PG synthesis. Both strains showed labeling at the base of the stalk. Scale bars: 5 μm. (E) The indicated strains were streaked onto HIGG plates supplemented with 3% sucrose to induce EPS production and mucoidy. Wild-type cells had a distinct mucoid appearance whereas *manA** was matte in appearance signifying a decrease in EPS production. CB15 and NA1000 ΔMGE (EK717) were non-EPS-producing control strains. (F) The indicated strains were grown in HIGG-1 μM phosphate for 48 h and stalk lengths were measured using ImageJ (error bars are SEM, ANOVA $F(4,377)=115.5$, $P<0.0001$; * post-hoc comparisons using Bonferroni test, $P<0.05$). The Tn5::*wbqP* strain, which does not make O-antigen, had a partial effect on stalk elongation compared to the *manA** strain. The effect of the *wbqP* transposon insertion was fully complemented by inducible expression of *wbqP*.

Figure 4. *manA cells have a defect in stationary-phase entry which contributes to the stalk-elongation phenotype.** (A) Metabolomic analyses of wild-type and *manA** (KD145) cells grown in HIGG- 1 μM phosphate demonstrated that wild-type cells have higher levels of M6P as well as TCA cycle metabolites. The horizontal lines indicate a 1.5-fold difference between wild-type

and *manA**. Bars are the means of 3 independent experiments. (B) Growth curves of wild-type, *manA**, and complemented *manA** cells in HIGG- 30 μM phosphate showed that *manA** grows to a higher OD than wild-type (error bars are SEM, n=3). (C) WT and *manA** cells were grown in HIGG- 1 μM phosphate for 72 h prior to imaging. Scale bar: 5 μm. (D) Wild-type and *manA** cells were grown in HIGG-30 μM phosphate for 48 h. Wild-type and *manA** cultures were back diluted into HIGG-30 μM phosphate to an OD_{660} = 0.03 and allowed to grow for 48 h. Expression of the indicated stationary-phase genes was measured by qRT-PCR and relative mRNA levels between wild-type and *manA** were quantified. Gene expression was normalized to *rpoH* mRNA (error bars are SEM, n=3). (E) Wild-type and Δ*spdR* (KD181) cells were grown for 48 h in HIGG- 1 μM phosphate and stalk lengths were measured. *spdR* deletion inhibits stalk elongation (error bars are SEM, * Mann-Whitney U=2778, n_1=58, n_2=61, $P < 0.05$ two-tailed). (F) *manA** cells with or without exogenous expression of constitutively-active RelA (KD178) were grown in HIGG- 1 μM phosphate with 0.003% xylose and stalk length was measured by microscopy (error bars are SEM, * Mann-Whitney U=1313, n_1=70, n_2=87, $P < 0.05$ two-tailed).

Figure 1

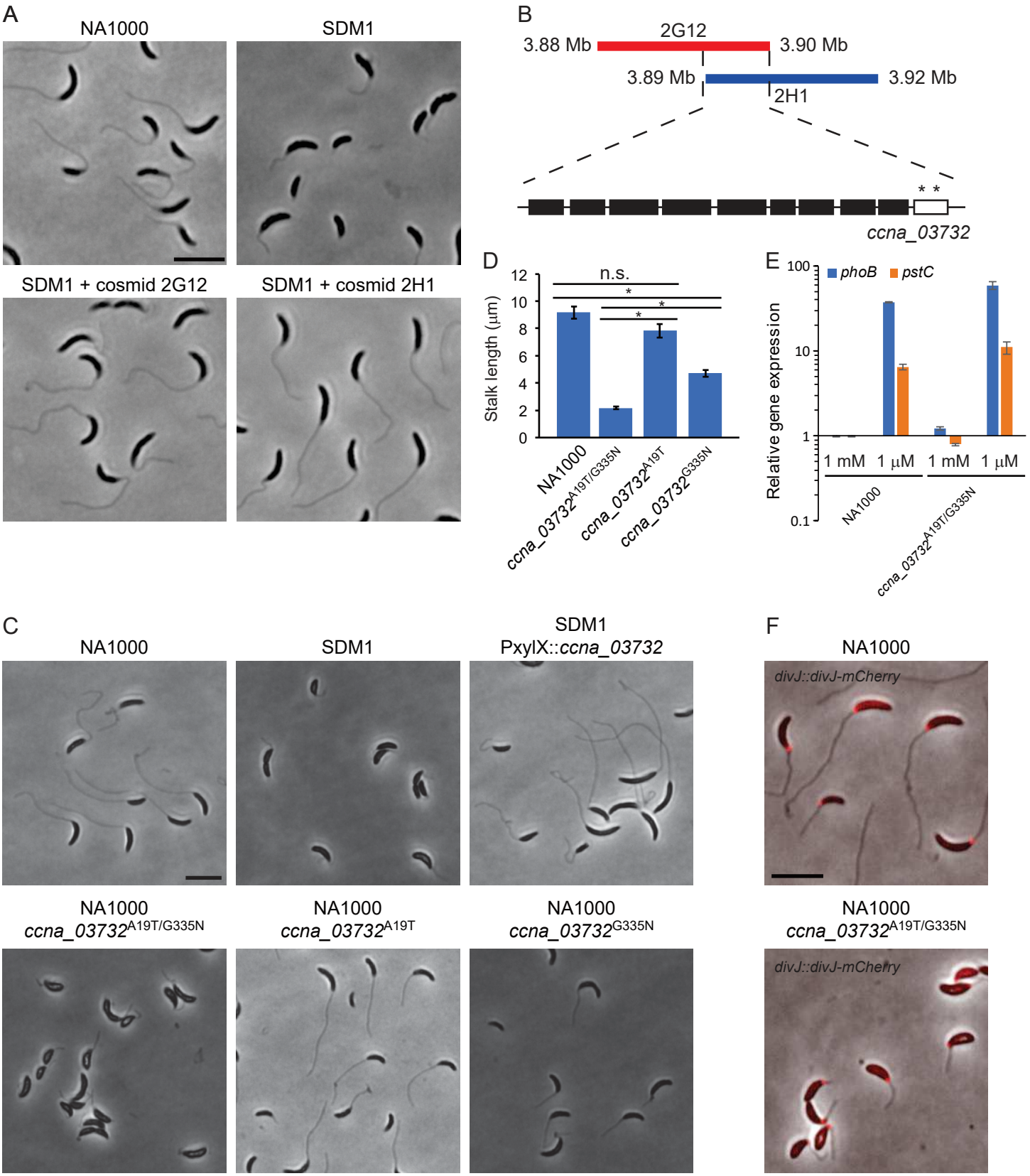
A
NA1000
SDM1
SDM1 + cosmid 2G12
SDM1 + cosmid 2H1
B
2G12
3.88 Mb
3.90 Mb
3.89 Mb
3.92 Mb
2H1
ccna_03732
D
n.s.
Stalk length (μm)
NA1000
ccna_03732A19T/G335N
ccna_03732A19T
ccna_03732G335N
E
phoB
pstC
Relative gene expression
1 mM
1 μM
1 mM
1 μM
NA1000
ccna_03732A19T/G335N
C
NA1000
SDM1
SDM1
PxylX::ccna_03732
NA1000
ccna_03732A19T/G335N
NA1000
ccna_03732A19T
NA1000
ccna_03732G335N
F
NA1000
divJ::divJ-mCherry
NA1000
ccna_03732A19T/G335N
divJ::divJ-mCherry

Figure 2

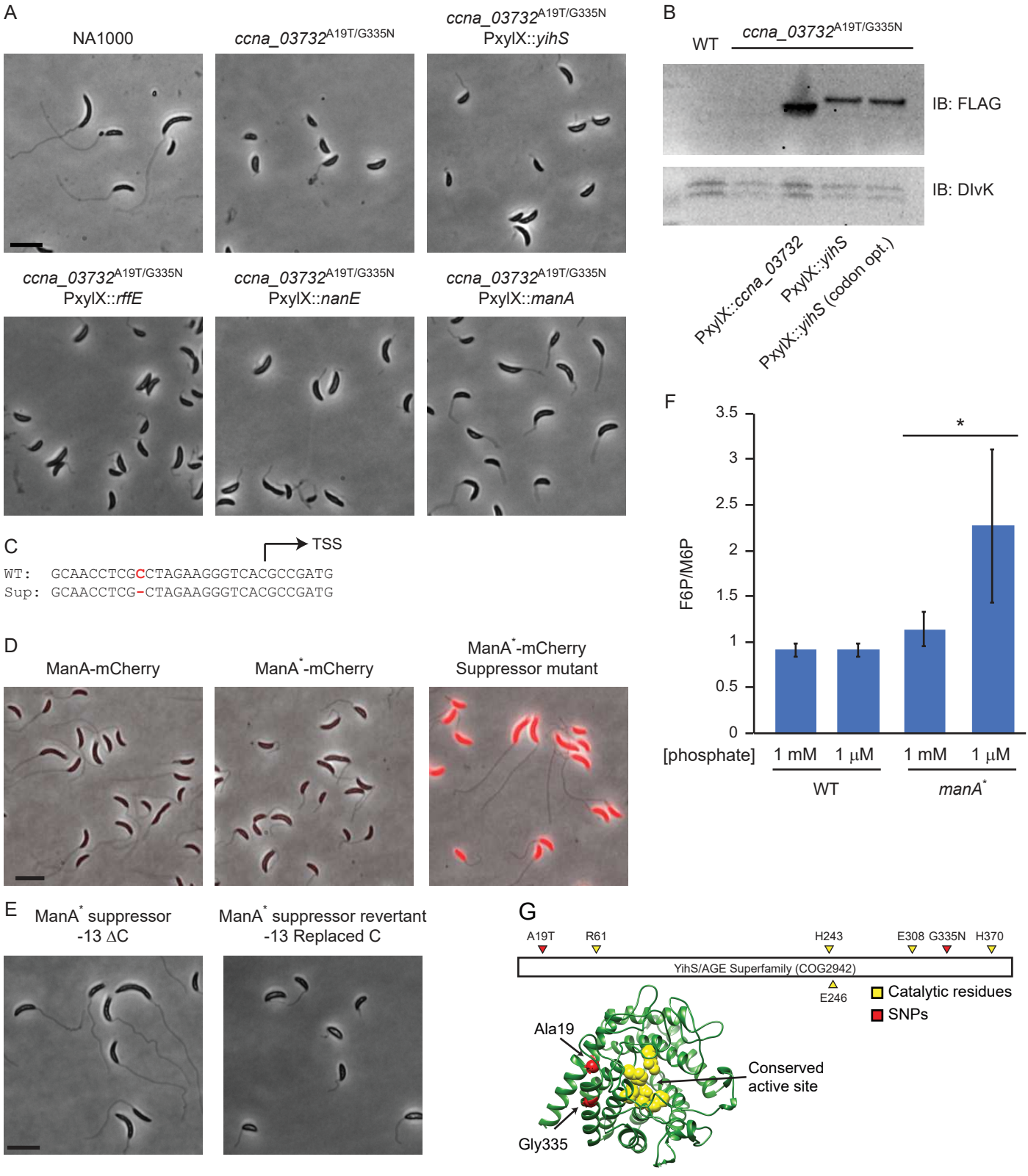
A
NA1000
ccna_03732A19T/G335N
ccna_03732A19T/G335N PxylX::yihS
ccna_03732A19T/G335N PxylX::rffE
ccna_03732A19T/G335N PxylX::nanE
ccna_03732A19T/G335N PxylX::manA
B
WT
ccna_03732A19T/G335N
IB: FLAG
IB: DlvK
PxylX::ccna_03732
PxylX::yihS
PxylX::yihS (codon opt.)
C
TSS
WT: GCAACCTCGCCTAGAAGGGTCACGCCGATG
Sup: GCAACCTCG-CTAGAAGGGTCACGCCGATG
D
ManA-mCherry
ManA*-mCherry
ManA*-mCherry Suppressor mutant
E
ManA* suppressor -13 ΔC
ManA* suppressor revertant -13 Replaced C
F
F6P/M6P
3.5
3
2.5
2
1.5
1
0.5
0
*
[phosphate]
1 mM
1 μM
1 mM
1 μM
WT
manA*
G
A19T
R61
H243
E308
G335N
H370
YihS/AGE Superfamily (COG2942)
E246
Catalytic residues
SNPs
Ala19
Conserved active site
Gly335

Figure 3

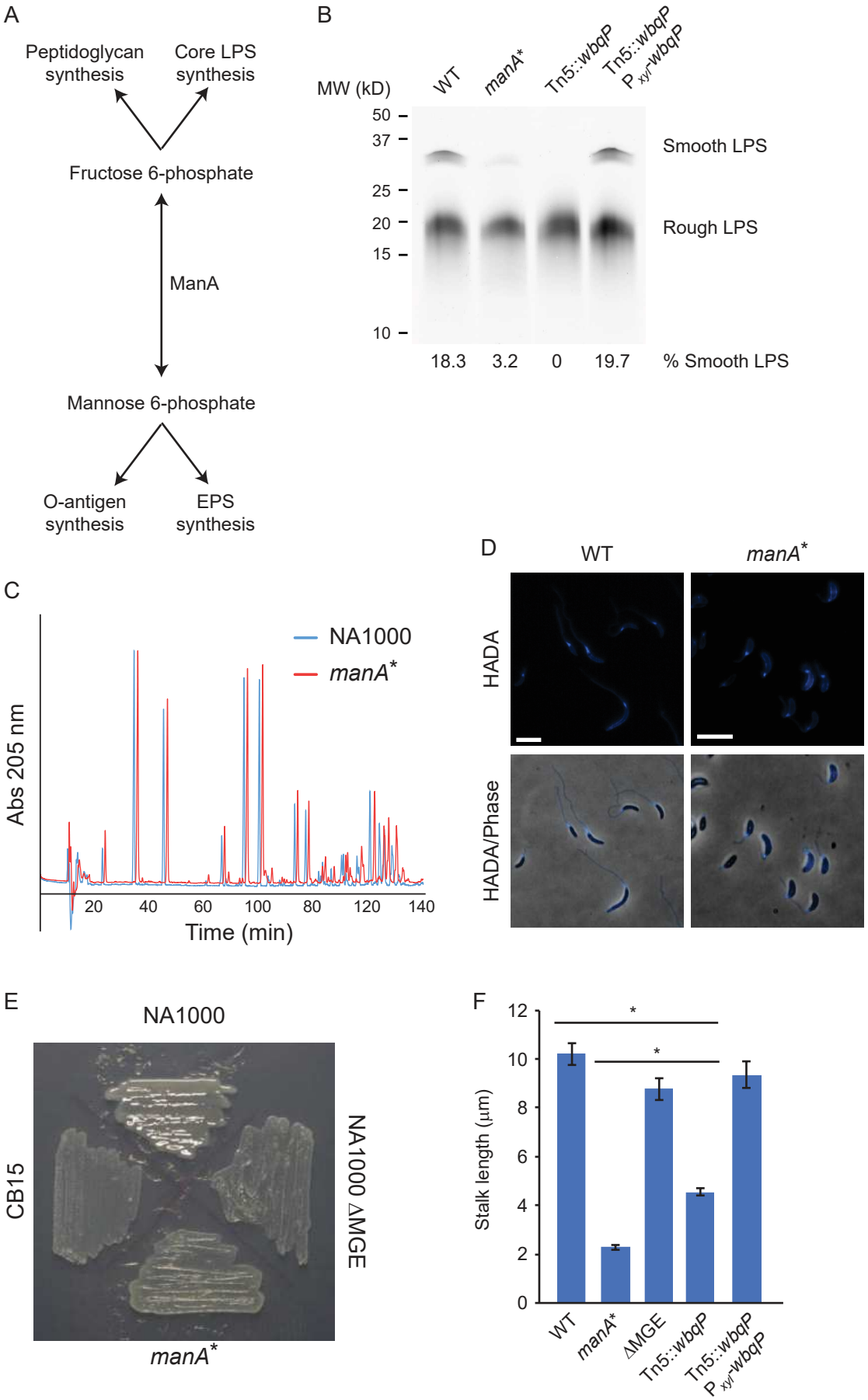
A
Peptidoglycan synthesis
Core LPS synthesis
Fructose 6-phosphate
ManA
Mannose 6-phosphate
O-antigen synthesis
EPS synthesis
B
MW (kD)
WT
manA*
Tn5::wbqP
Tn5::wbqP Pxyl-wbqP
50
37
25
20
15
10
Smooth LPS
Rough LPS
18.3
3.2
0
19.7
% Smooth LPS
C
NA1000
manA*
Abs 205 nm
20
40
60
100
80
120
140
Time (min)
D
WT
manA*
HADA
HADA/Phase
E
NA1000
CB15
NA1000 ΔMGE
manA*
F
Stalk length (μm)
12
10
8
6
4
2
0
*
*
WT
manA*
ΔMGE
Tn5::wbqP
Tn5::wbqP Pxyl-wbqP

Figure 4

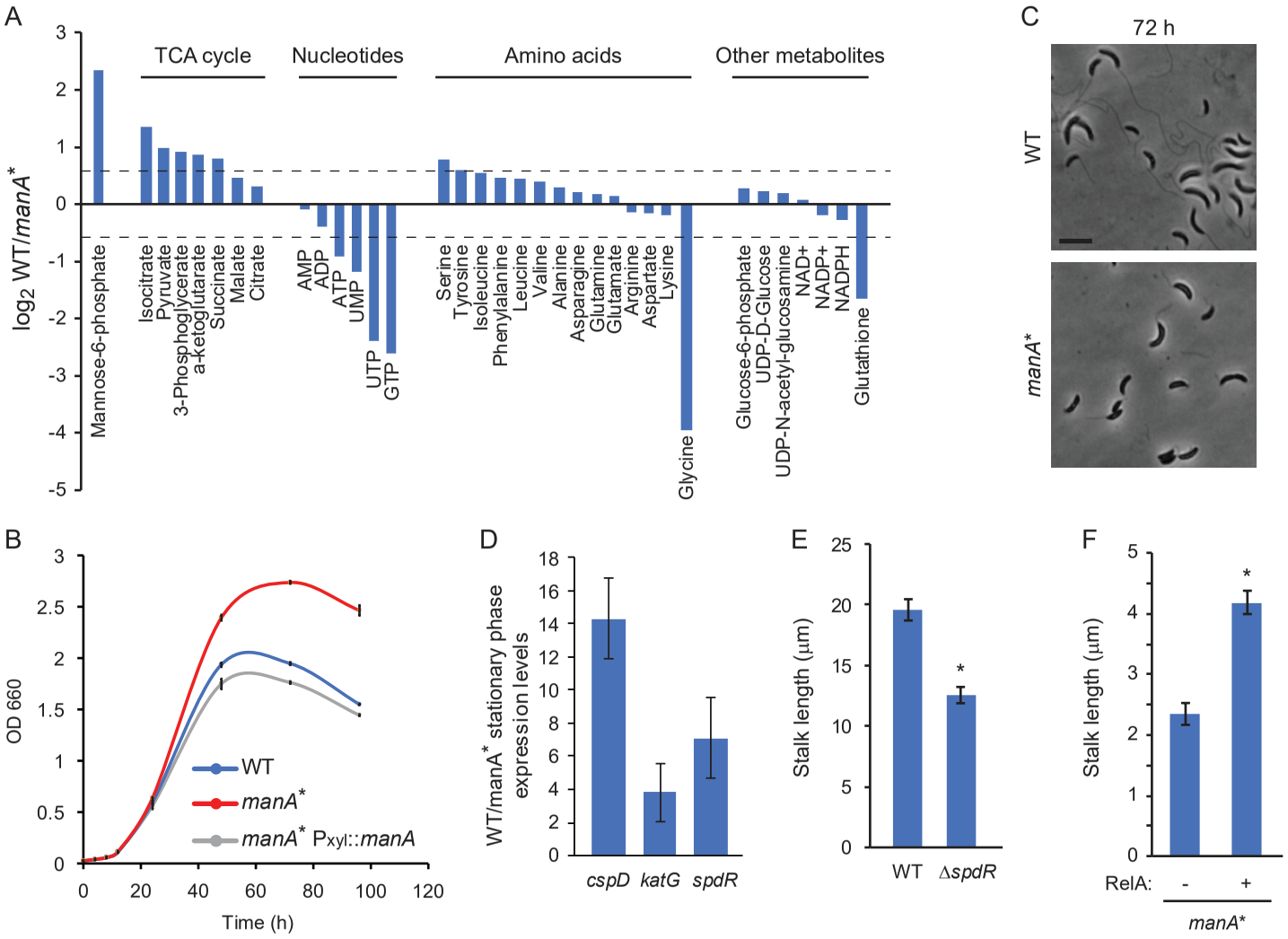
A
TCA cycle
Nucleotides
Amino acids
Other metabolites
log2 WT/manA*
Mannose-6-phosphate
Isocitrate
Pyruvate
3-Phosphoglycerate
a-ketoglutarate
Succinate
Malate
Citrate
AMP
ADP
ATP
UMP
UTP
GTP
Serine
Tyrosine
Isoleucine
Phenylalanine
Leucine
Valine
Alanine
Asparagine
Glutamine
Glutamate
Arginine
Aspartate
Lysine
Glycine
Glucose-6-phosphate
UDP-D-Glucose
UDP-N-acetyl-glucosamine
NAD+
NADP+
NADPH
Glutathione
C
72 h
WT
manA*
B
OD 660
Time (h)
WT
manA*
manA* Pxyl::manA
D
WT/manA* stationary phase expression levels
cspD
katG
spdR
E
Stalk length (μm)
WT
ΔspdR
F
Stalk length (μm)
RelA:
manA*